Ab initio calculation of the phase stability in Au-Pd and Ag-Pt alloys

Marcel H. F. Sluiter*
Department of Materials Science and Engineering, Delft University of Technology, Mekelweg 2, 2628CD Delft, The Netherlands

C. Colinet
Laboratoire de Thermodynamique et Physico-Chimie Métallurgiques, Saint Martin d'Hères, France

Alain Pasturel
Laboratoire de Physique et Modélisation des Milieux Condensés, Maison des magistères Boîte Postale 166 CNRS, 38042 Grenoble-Cedex 09, France

(Received 12 January 2006; revised manuscript received 13 March 2006; published 5 May 2006)

The phase stability of superstructures based on the fcc lattice in the Au-Pd and Ag-Pt alloy systems are examined from the fully relativistic electronic density functional theory. The electron-ion interaction is described by the projector augmented-wave (PAW) method and the exchange-correlation effects are treated in the generalized gradient approximation (GGA). The cluster expansion method is used to obtain effective cluster interactions on the fcc lattice and is used also to guide a systematic ground state search for both alloy systems. The ground state analysis reveals a multitude of ground states in Au-Pd, especially at the Au-rich side. Possibly long-period super-structures occur near the $Au_{70}Pd_{30}$ composition. The ground state analysis indicates a uniquely stable AgPt compound with the $L1_1$ structure (CuPt prototype) and it also suggests a marginally stable ordered compound for Ag_3Pt. However, our *ab initio* study rules out the existence of the remarkably stable Ag_3Pt phase with $L1_2$ structure, reported first more than half a century ago and since then included in many assessments. We also find no indication for a stable ordered state at the $AgPt_3$ composition. The cluster variation method (CVM) with a large maximal cluster is used to compute the enthalpy of mixing of the disordered solid solutions and the solid portion of the Au-Pd and Ag-Pt phase diagrams. These results are critically compared with experimental data and phase diagram assessments. It is shown that cluster expansions cannot account for the high-temperature miscibility gap in the Ag-Pt system when the effective cluster interactions do not reach beyond the second nearest neighbor. Only when third nearest neighbors are included in the cluster expansion is it possible to obtain a phase diagram that agrees qualitatively with the assessed Ag-Pt phase diagram.

DOI: 10.1103/PhysRevB.73.174204 PACS number(s): 61.66.Dk, 64.75.+g, 82.60.Lf, 71.20.Lp

I. INTRODUCTION

The alloys A-B with A=Cu, Ag, Au and B=Ni, Pd, Pt possess the same number of valence electrons per atom. However, their phase diagrams show dissimilarities.[1] At first sight, one would suspect that the small differences in electronegativity between the A and B elements and the almost complete filling of the *d*-band might give weak chemical affinity so that atomic size effects dominate the tendencies towards ordering and phase separation. However, a brief summary of the main features of the phase diagrams shows that this is an oversimplification.

The three diagrams with nickel as one constituent feature a miscibility gap, the critical temperature is 354.5 °C in the Cu-Ni system, 810.3 °C in the Au-Ni system, and is above the liquidus temperature in the Ag-Ni system. The three diagrams with palladium show an extended fcc solid solution below the liquidus line. The Cu-Pd system exhibits ordered phases at low temperature, although it must be emphasized that a bcc superstructure, the B2 structure (CsCl prototype), is the ground state at equiatomic composition. Moreover, the fcc based long-period superstructures have been observed around the Cu_3Pd composition. In the case of the Ag-Pd system, no superstructures have been observed experimentally at low temperature. The phase diagram of the Au-Pd system has ordered $L1_2$ structures for Au_3Pd and $AuPd_3$ compositions, while for the equiatomic composition the structure has not been determined,[2,3] see Fig. 1.

The phase diagrams based on platinum have various features. The Cu-Pt phase diagram exhibits an extended fcc solid solution below the liquidus line. At lower temperature, the $L1_1$ and $L1_2$ superstructures have been observed for the Cu-Pt and Cu_3Pt compositions, respectively. The CuPt structure, often considered unique, is similar to HgIn, LiPb, and FeO prototype structures. In spite of a 100 year history and many studies,[4–10] the Ag-Pt system is not well understood. The Ag-Pt phase diagram assessed by Karakaya and Thompson[9,11] displays superstructures at low temperature (most not clearly identified) and a miscibility gap between a silver-rich solid solution and a platinum-rich solid solution at higher temperature, the critical temperature being higher than the liquidus temperature. Recently Durussel and Feschott[10] revised completely the Ag-Pt phase diagram using differential thermal analysis, x-ray diffraction and electron microprobe analysis on long-time annealed specimens, see Fig. 2. They confirmed the presence of the equilibrium between two solid solutions a silver rich solid solution and a platinum rich solid solution, but they also detected the pres-

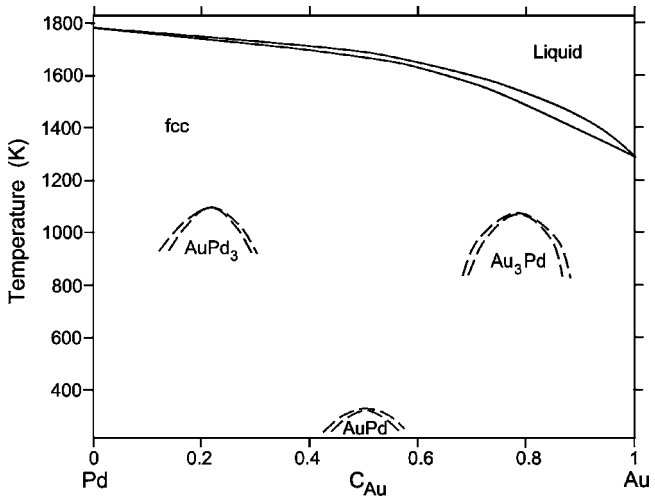

FIG. 1. Au-Pd phase diagram redrawn from Ref. 3 which is an assessment of the experimental data. Dashed lines are speculative.

ence of an intermediate phase $Ag_{15}Pt_{17}$ which decomposes by a peritectoid transformation in the two solid solutions at 803 °C. They could not give the crystal structure of the intermediate phase but suggested it is a deformed cubic structure corresponding to 32 atoms per cell. Very recently Erni *et al.*[12] performed transmission electron microscopy of an $Ag_{85}Pt_{15}$ alloy and concluded that the phase Ag_3Pt with $L1_2$ structure, reported first more than half a century ago[6] and since then included in many assessments, does not exist. For the last system in the series, Au-Pt, the phase diagram presents a miscibility gap in the solid state with a critical temperature of 1260 °C just below the solid-liquid equilibrium.

From a theoretical point of view, a systematic study of the nine systems has been performed by Takizawa *et al.*[13] using the augmented spherical wave (ASW) method including the relativistic effects except the spin-orbit interaction. The total energy calculations were performed for three structures $L1_2$ (A_3B and AB_3) and $L1_0$ (AB). In some cases other structures as B2 (AB) and $L1_1$ (AB) were studied. These authors confirmed the positive values of the enthalpies of mixing in the Ni based systems and, therefore, diagrams displaying a miscibility gap. In the Cu-Pd system, Takizawa *et al.*[13] found that for CuPd the B2 structure is more stable than $L1_0$ and $L1_1$ structures. It was also predicted that the $L1_1$ structure is more stable than the $L1_0$ structure in the Ag-Pd and Cu-Pt systems for the equiatomic composition and that both Ag-Pt and Au-Pt systems phase separate.[13] Later the same authors[14–17] extensively studied the Au-Pd system, considering the $L1_0$ structure at equiatomic composition.

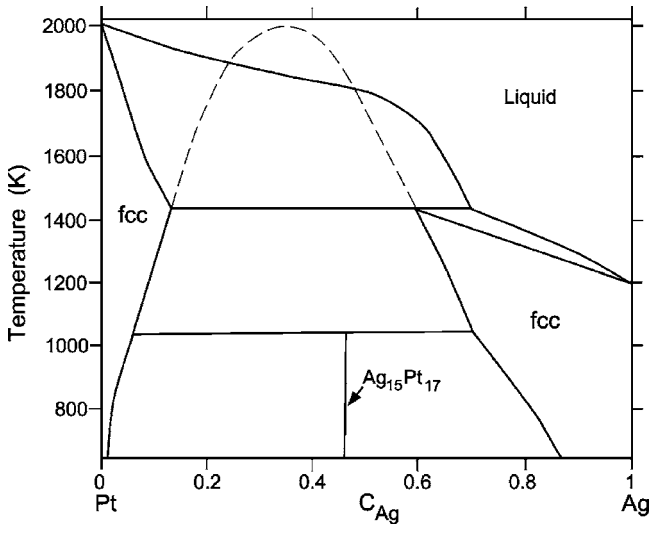

FIG. 2. Ag-Pt phase diagram based on the assessed experimental phase diagram from Ref. 10. Dashed line schematically represents the extrapolated hypothetical miscibility gap in the fcc solid solution.

Further studies, confirming the general trends obtained by Takizawa *et al.*,[13] were performed using the full potential linear augmented planewave method (FLAPW) or the full potential linear muffin tin method (FPLMTO). These studies concern the systems Cu-Ni and Ag-Ni,[18] Au-Ni,[19–26] Cu-Pd,[27–34] Ag-Pd,[35,36] Cu-Pt,[27] and Au-Pt.[19] Recent calculations performed by Müller and Zunger[36] confirmed that the $L1_1$ superstructure is the ground state at equiatomic composition in the Ag-Pd system, and these authors found that a new superstructure called $L1_1^+$ is the ground state for the $AgPd_3$ composition. In the Au-Pd system, Weinberger *et al.*[37,38] used the Korringa-Kohn-Rostoker coherent potential approximation method to obtain the enthalpy of mixing of the disordered solid solution[38] and the effective pair interactions up to the fifth nearest neighbors.[37] Abrikosov and Skriver[39] obtained the enthalpies of mixing of random Cu-Ni, Ag-Pd, and Au-Pt alloys using the coherent potential approximation within a tight binding linear muffin-tin orbitals basis. Their results are in good agreement with both experimental and other theoretical data.

In the present work, we will focus our attention on two systems Au-Pd and Ag-Pt. Although there are strong similarities between the two systems, such as Pauling electronegativity differences of 0.34 and 0.35, and atomic volume differences of 14% and 12%, respectively, no phase separation tendencies are reported for the Au-Pd system while the evidence for these tendencies in Ag-Pt appears irrefutable. In the Au-Pd system, it is well established that the system orders at low temperature. However, two points deserve to be clarified: (a) What are the superstructures formed at low temperature? The theoretical work performed by Weinberger *et al.*[37,38] indicates that the structures in the Au-Pd system are not of the $\langle 100 \rangle$ ordering type such as $L1_0$ and $L1_2$, but rather belong to the $\langle \frac{1}{2}\frac{1}{2}\frac{1}{2} \rangle$ family such as the $L1_1$ (CuPt prototype) type structure with a possibility of finding $\langle 1\frac{1}{2}0 \rangle$ type structures such as $D0_{22}$ (Al_3Ti prototype) and type 40 (UPb prototype[40]) structures.[41] (b) What is the order of magnitude of the order-disorder temperatures? Rather high order-disorder temperatures are reported in the experimental phase diagram for the Au_3Pd and $AuPd_3$ compositions (850 °C and 870 °C, respectively) while for the equiatomic composition, this temperature is found to be much lower (100 °C). Weinberger *et al.*[38] found values for the mixing enthalpy about twice as large as those measured by Darby[42] and Hayes and Kubaschewski[43] or as calculated by Takizawa *et al.*[13]

In the Ag-Pt system, the theoretical work performed by Takizawa *et al.*[13] considered only three structures, $L1_2$ Ag_3Pt, $L1_0$ AgPt, and $L1_2$ $AgPt_3$ which are not sufficient to

explain the possible low temperature structures and the complexity of the phase diagram. The challenge is to perform a more complete ground state analysis on the fcc lattice in order to see if an fcc superstructure can be stabilized at low temperature while the miscibility gap which exists at higher temperatures must be explained.

Our investigation is based on the electronic density functional theory (DFT) calculations of selected superstructures based on the fcc lattice. These calculations have been performed with the Vienna *ab initio* simulation package (VASP).[44,45] The formation energies of the fcc superstructures are described by a generalized Ising Hamiltonian[46–48] and a ground state search is performed considering all possible structures with primitive translations corresponding to pairs up to and including the sixth nearest neighbor (the fcc cube body diagonal) and having 16 atoms in the cell or fewer. An optimal cluster expansion (CE) was obtained by direct enumeration of all possible invariant[49] CEs up to a certain limited number of terms. The CE is introduced in the CVM[48,50–52] in order to get the enthalpy and entropy of mixing as function of temperature and finally to compute the fcc phase diagram.

The outline of the paper is as follows. In Sec. II, we describe the computational methods. Section III is devoted to the results of the *ab initio* calculations of the formation enthalpies of fcc superstructures in the Au-Pd and Ag-Pt systems. Section IV presents the results of the CE and the ground state search. In Sec. V, the Au-Pd and Ag-Pt fcc phase diagrams are computed using the CVM. Our conclusions are presented in Sec. VI.

II. COMPUTATIONAL METHOD

The zero temperature thermodynamic and structural parameters were calculated with the electronic density functional theory where the electron-electron many body effects are parametrized as a functional of the charge density in the so-called generalized gradient approximation (GGA). In the present work, the generalized gradient corrected version in the form of the Perdew-Wang[53,54] functional is used to obtain the one-electron Hamiltonian. We used the most recent version of VASP[44,45] in which the interaction between the ions and electrons is described by the projector augmented-wave method[55] implemented by Kresse and Joubert.[56] The calculations include $4d^{10}\,5s^1$, $5d^{10}\,6s^1$, $4d^9\,5s^1$, $5d^9\,6s^1$ valence electrons with a default plane-wave cutoff for the representation of the wave functions of 250, 230, 350, 230 eV for Ag, Au, Pd, and Pt, respectively. This means that for the binary alloys the higher of the cutoffs is relevant only: 250 eV for Ag-Pt and 350 eV for Au-Pd. The Brillouin-zone integration is performed with Monkhorst-Pack grids[57] using the Methfessel-Paxton[58] technique, a generalized Gaussian smearing method, with a modest smearing of the one-electron levels (0.1 eV) for better structural relaxations.

To attain the best cancellation of systematic errors in the formation energies of the fcc superstructures, we used the same high numerical precision in all calculations, including the use of geometrically equivalent k points where possible, identical integration schemes and basis sets. The calculations of the Hellmann-Feynman forces acting on the atoms and of the stresses on the unit cell enabled optimization of the total energy with respect to volume, cell shape, and internal structural parameters (i.e., the local displacements of the basis atoms away form the ideal fcc lattice sites). The fcc superstructures[27,41,47,59–62] for which total energy calculations have been performed are reported in Table I. It is important to consider the space-group of a structure in order to know which external and internal relaxations are allowed. Therefore, in columns 6 and 7 of Table I, we have reported the conditions for which the atoms are on the fcc lattice, these columns also permit to look at the allowed relaxations with respect to this lattice. Many of the superstructures can be considered as A_mB_n superlattices along a particular direction.[27] When such an interpretation is possible, the wave vector is listed in the last column of Table I. The wave vectors can be used to classify and group superstructures see, e.g., Ref. 63. Moreover, with knowledge of the ordering wave vectors, the Landau rules can be used to determine the order of phase transitions between the solid solution and the superstructures, and, as is the case here, when the superstructures are all based on the same parent lattice they can be used even for transformations between the superstructures themselves.[64]

We have also performed PAW calculations of the total energies of special quasirandom structures (SQSs) with eight atoms/cell.[65] These structures are designed to mimic perfectly random structures by reproducing random behavior for the near neighbors around each site, deferring periodicity errors to more distant neighbors and clusters involving many atoms. Descriptions of these SQSs may be found also in (Refs. 29 and 35).

III. RESULTS OF THE *AB INITIO* CALCULATIONS

The formation enthalpy ΔH_f (at zero pressure) is obtained by subtracting the concentration weighted enthalpy of pure fcc Au (Ag) and Pd (Pt):

$$\Delta H_f(Au_{1-x}Pd_x) = H(Au_{1-x}Pd_x) - [(1-x)H(Au) + xH(Pd)]. \quad (1)$$

Whether a system will form compounds or phase separate in the pure elements is determined by the sign of the formation enthalpy. In Tables II and III, we report the formation enthalpies of all fcc superstructures considered for the Au-Pd and Ag-Pt systems, respectively.

Au-Pd system exhibits negative formation enthalpies for all the structures studied, thus unequivocally indicating ordering rather than phase separating tendencies. Ag-Pt system displays a peculiar behavior; although the formation enthalpies are positive for the majority of the studied structures, a few structures display negative formation enthalpies. Because Weinberger *et al.*[37,38] performed fully relativistic calculations in the Au-Pd system, we have checked the influence of such an approximation by performing a series of calculations for both systems, including the spin-orbit treatment following Le Bacq and Kresse's prescriptions.[66] The maximum difference obtained between the two sets of calculations is less than 3 meV/atom and we can safely assume

TABLE I. Crystallographic description of the fcc superstructures.

Compound	Pearson symbol	Prototype	Strukturbericht designation	Space group number	Lattice parameters	Positions	Superlattice directions
A or B	cF4	Cu	A1	$Fm\bar{3}m$, 225	a_{fcc}	A 4*a* $x=0$, $y=0$, $z=0$	
AB	tP2	AuCu	$L1_0$	P4/mmm, 123	$a_t=a_{fcc}$	A 1*a* $x=0$, $y=0$, $z=0$	AB along [001] and [110]
					$c_t=a_{fcc}$	B 1*d* $x=1/2$, $y=1/2$, $z=1/2$	
AB	tI8	UPb	40[a]	$I4_1/amd$, 141	$a_t=a_{fcc}$	A 4*a* $x=0$, $y=0$, $z=0$	A_2B_2 along [012]
					$c_t=2a_{fcc}$	B 4*b* $x=0$, $y=0$, $z=1/2$	
AB	hR32	CuPt	$L1_1$	$R\bar{3}m$, 166	$a_r=\sqrt{3/2}a_{fcc}$	A 1*a* $x=0$, $y=0$, $z=0$	AB along [111] and [311]
					$b_r=\sqrt{3/2}a_{fcc}$	B 1*b* $x=1$, $y=1$, $z=1$	
					$\Theta=17.34°$		
AB	cF32		D4[b]	$Fd\bar{3}m$, 227	$a=2a_{fcc}$	A 16*c* $x=0$, $y=0$, $z=0$	none
						B 16*d* $x=1/2$, $y=1/2$, $z=1/2$	
AB	tP4		Z2[b,c]	P4/nmm, 129	$a_t=\sqrt{1/2}a_{fcc}$	A 2*c* $x=-1/4$, $y=1/4$, $z=1/8$	A_2B_2 along [001]
					$c_t=2a_{fcc}$	B 2*c* $x=-1/4$, $y=1/4$, $z=5/8$	
AB	oP4		Y2[b]	Pmmn, 59	$a_o=\sqrt{5/2}a_{fcc}$	A 2*a* $x=0$, $y=0$, $z=1/8$	A_2B_2 along [110]
					$b_o=a_{fcc}$	B 2*a* $x=0$, $y=0$, $z=-3/8$	
					$c_o=\sqrt{2}a_{fcc}$		
AB	hR4		V2[b]	$R\bar{3}m$, 166	$a_r=\sqrt{11/2}a_{fcc}$	A 2*c* $x=y=z=-1/8$	A_2B_2 along [111]
					$b_r=\sqrt{11/2}a_{fcc}$	B 2*c* $x=y=z=3/8$	
					$\Theta=17.34°$		
A_2B	oI6	$MoPt_2$		Immm, 71	$a_o=\sqrt{1/2}a_{fcc}$	A 4*g* $x=0$, $y=1/3$, $z=0$	A_2B along [110]
					$b_o=\sqrt{9/2}a_{fcc}$	B 2*a* $x=0$, $y=0$, $z=0$	
					$c_o=a_{fcc}$		
A_2B	tI6		β[b,d]	I4/mmm, 139	$a_t=\sqrt{1/2}a_{fcc}$	A 4*e* $x=0$, $y=0$, $z=1/3$	A_2B along [001]
					$c_t=3a_{fcc}$	B 2*a* $x=0$, $y=0$, $z=0$	
A_2B	hP3	CdI_2	C6	$P\bar{3}m1$, 164	$a_h=\sqrt{1/2}a_{fcc}$	A 2*d* $x=1/3$, $y=2/3$, $z=-1/3$	A_2B along [111]
					$c_h=\sqrt{3}a_{fcc}$	B 1*a* $x=0$, $y=0$, $z=0$	
A_2B	mC12			C2/m, 12	$a_m=\sqrt{3/2}a_{fcc}$	A 4*g* $x=0$, $y=1/6$, $z=0$	none
					$b_m=\sqrt{3/2}a_{fcc}$	A 4*h* $x=0$, $y=1/3$, $z=1/2$	
					$c_m=\sqrt{11/2}a_{fcc}$	B 2*b* $x=1/2$, $y=0$, $z=0$	
					$\Theta=115.8°$	B 2*c* $x=0$, $y=0$, $z=1/2$	
A_5B_2	mC14	Mn_2Au_5		C2/m, 12	$a_m=\sqrt{5}a_{fcc}$	A 2*a* $x=0$, $y=0$, $z=0$	
					$b_m=a_{fcc}$	A 4*i* $x=0.143$, $y=0$, $z=0.429$	
					$c_m=\sqrt{5/2}a_{fcc}$	A 4*i* $x=0.714$, $y=0$, $z=0.143$	
					$\Theta=98.13°$	B 4*i* $x=0.429$, $y=0$, $z=0.286$	
A_3B	cP4	$AuCu_3$	$L1_2$	$Pm\bar{3}m$, 221	a_{fcc}	A 3*c* $x=0$, $y=1/2$, $z=1/2$	none
						B 1*a* $x=0$, $y=0$, $z=0$	
A_3B	tI8	Al_3Ti	$D0_{22}$	I4/mmm, 139	$a_t=a_{fcc}$	A 2*b* $x=0$, $y=0$, $z=1/2$	A_3B along [012]
					$c_t=2a_{fcc}$	A 4*d* $x=1/2$, $y=0$, $z=1/4$	
						B 2*a* $x=0$, $y=0$, $z=0$	
A_3B	tP4		Z1[b]	P4/mmm, 123	$a_t=\sqrt{1/2}a_{fcc}$	A 1*d* $x=1/2$, $y=1/2$, $z=1/2$	A_3B along [001]
					$c_t=2a_{fcc}$	A 2*g* $x=0$, $y=0$, $z=1/4$	
						B 1*c* $x=1/2$, $y=1/2$, $z=0$	
A_3B	oP4		Y1[b]	Pmmm, 47	$a_o=\sqrt{5/2}a_{fcc}$	A 2*i* $x=-1/4$, $y=0$, $z=0$	A_3B along [110]
					$b_o=a_{fcc}$	A 1*h* $x=1/2$, $y=1/2$, $z=1/2$	
					$c_o=\sqrt{2}a_{fcc}$	B 1*g* $x=0$, $y=1/2$, $z=1/2$	
A_3B	hR4		V1[b]	$R\bar{3}m$, 166	$a_r=\sqrt{11/2}a_{fcc}$	A 2*c* $x=y=z=1/4$	A'_3B along [111]
					$b_r=\sqrt{11/2}a_{fcc}$	A 1*b* $x=1/2$, $y=1/2$, $z=1/2$	

TABLE I. (*Continued.*)

Compound	Pearson symbol	Prototype	Strukturbericht designation	Space group number	Lattice parameters	Positions	Superlattice directions
					$\Theta=17.34°$	B $1a$ $x=0$, $y=0$, $z=0$	
A_3B	oC8		$L1_1^+$[e]	Cmmm, 65	$a_o=2a_{fcc}$	A $2b$ $x=1/2$, $y=0$, $z=0$	$A/A_{0.5}B_{0.5}$ along [111]
					$b_o=\sqrt{2}a_{fcc}$	A $4f$ $x=1/4$, $y=1/4$, $z=1/2$	
					$c_o=\sqrt{1/2}a_{fcc}$	B $2a$ $x=0$, $y=0$, $z=0$	
A_4B	tI10	$MoNi_4$	$D1_a$	I4/m, 87	$a_t=\sqrt{5/2}a_{fcc}$	A $8h$ $x=2/5$ $y=1/5$, $z=0$	A_4B along [103]
					$c_t=a_{fcc}$	B $2a$ $x=0$, $y=0$, $z=0$	
A_5B	mC12			C2/m, 12	$a_m=\sqrt{3/2}a_{fcc}$	A $4g$ $x=0$, $y=1/6$, $z=0$	none
					$b_m=\sqrt{3/2}a_{fcc}$	A $4h$ $x=0$, $y=1/3$, $z=1/2$	
					$c_m=\sqrt{11/2}a_{fcc}$	A $2c$ $x=0$, $y=0$, $z=1/2$	
					$\Theta=115.8°$	B $2b$ $x=1/2$, $y=0$, $z=0$	
A_7B	cF32	Ca_7Ge	D1, D7[b]	$Fm\bar{3}m$, 225	$a=2a_{fcc}$	A $4b$ $x=1/2$, $y=1/2$, $z=1/2$	none
						A $24d$ $x=0$, $y=1/4$, $z=1/4$	
						B $4a$ $x=0$, $y=0$, $z=0$	
A_8B	tI18	$NbNi_8$		I4/mmm, 139	$a_t=\sqrt{9/2}a_{fcc}$	A $8h$ $x=1/3$, $y=1/3$, $z=0$	none
					$c_t=a_{fcc}$	A $8i$ $x=1/3$, $y=0$, $z=0$	
						B $2a$ $x=0$, $y=0$, $z=0$	

[a]Named by Kanamori and Kakehashi (Ref. 41), UPb prototype (Ref. 40).
[b]Named by Lu *et al.*, Ref. 27.
[c]Bain distorted $B11$ (CuTi prototype).
[d]Bain distorted $C11_b$ ($MoSi_2$ prototype).
[e]Named by Müller and Zunger, Ref. 33.

that this effect need not be taken into account to determine the ground states in the Au-Pd and Ag-Pt systems.[67]

Although the formation enthalpies of Au-Pd and Ag-Pt systems take small values, there are important differences between the two systems. This difference cannot be explained on the basis on simple arguments like the size mismatch because Au-Pd and Ag-Pt have very similar atomic size differences: 14% in the case of Au-Pd and 12% in the case of Ag-Pt. The rather minor role of size mismatch is confirmed also by the small relaxation enthalpies which are typically an order of magnitude smaller than the formation enthalpies. For instance, in the Au-Pd system, the largest relaxation enthalpy has been obtained for the Z2 AuPd structure and it is just −14.5 meV/atom. Phenomenological theories are not conclusive on whether Au-Pd and Ag-Pt should phase-separate or order: Miedema's model[68] predicts $\Delta H_f = 0$ meV/atom for AuPd, −10 meV/atom for AgPt, 0 meV/atom for $AgPt_3$.[69] These values are not significant if one takes into account the limited accuracy of the model. Pettifor[70,71] predicts no ordered structures for Au-Pd at $x_{Au} = 0.5$ and 0.25, but Au_3Pd is predicted to take the $L1_2$ structure. In the Ag-Pt system, Pettifor[70,71] predicts the $L1_2$ structure for the Ag_3Pt and $AgPt_3$ compounds, and does not give any prediction at equiatomic composition. Johnson[72] used the embedded atom model to calculate the mixing enthalpy of random solid solution of noble metal based alloys. He obtained values near zero in the Au-Pd system and positive values in the Ag-Pt system (about 100 meV/atom at equiatomic composition). Moreover, as already mentioned above, the Ag-Pt system is very peculiar because the sign of the formation enthalpies of fcc superstructures depends on the symmetry of their crystallographic structures, emphasizing subtle effects in their electronic structures.

In Fig. 3 the formation enthalpies display a slight asymmetrical shape with respect to equiatomic composition, the more negative values occurring at the Au-rich side. Our calculated values of the formation enthalpies compare well with the values previously reported[13] for the $L1_2$ and $L1_0$ structures. For the equiatomic composition, the most stable structure is seen to be Nr. 40[41] (UPb prototype[40]). To the best of our knowledge, this structure has never been observed experimentally in metallic systems, but was found as a ground state in the Rh-Pt system by *ab initio* calculations.[28,62,73] Like Nr. 40, the other predicted structures such as Au_3Pd and $AuPd_3$ with $D0_{22}$ structures also belong to the $\langle 1\frac{1}{2}0\rangle$ family. However, the $D0_{22}$ $AuPd_3$ is almost degenerate in enthalpy with $L1_2$ $AuPd_3$. Additionally, the *ab initio* calculations find marginally stable $NbNi_8$ type Au_8Pd and Ni_4Mo type Au_4Pd. However, the latter two structures are only barely below the line connecting fcc Au and $D0_{22}$ Au_3Pd which means that they can be stable only at very low temperatures so that for practical purposes the Au_8Pd and Au_4Pd are not so relevant. The formation enthalpies of the SQSs are negative with the same asymmetrical shape with respect to the equiatomic composition as the formation enthalpies of the fcc superstructures.

Recently, Meschel and Kleppa[74] measured the heat of formation of the Au_3Pd compound by direct reaction calorimetry from room temperature to 1373 K and the heat content of the compound between 298 and 1373 K. They obtained a

TABLE II. Enthalpies of formation in meV/atom for fully relaxed fcc-based structures in the Au-Pd system as computed with the projector augmented planewave method.

Compound	Structure	ΔH_f	ΔH_f
Au, Pd	A1	0	0
Au_8Pd, $AuPd_8$	$NbNi_8$	−47	−20
Au_7Pd, $AuPd_7$	Ca_7Ge	−48	−23
Au_5Pd, $AuPd_5$	A_5B, C2/m	−62	−28
Au_4Pd, $AuPd_4$	$MoNi_4$	−82	−40
Au_3Pd, $AuPd_3$	$L1_2$	−97	−65
Au_3Pd, $AuPd_3$	$D0_{22}$	−101	−66
Au_3Pd, $AuPd_3$	$L1_1^+$	−81	−55
Au_3Pd, $AuPd_3$	V1	−54	−18
Au_3Pd, $AuPd_3$	Y1	−85	−45
Au_3Pd, $AuPd_3$	Z1	−70	−48
Au_3Pd, $AuPd_3$	SQS8	−82	−44
Au_5Pd_2, Au_2Pd_5	Mn_2Au_5	−101	−60
Au_2Pd, $AuPd_2$	$MoPt_2$	−104	−69
Au_2Pd, $AuPd_2$	β	−89	−61
Au_2Pd, $AuPd_2$	CdI_2	−69	−36
Au_2Pd, $AuPd_2$	A_2B, C2/m	−93	−59
AuPd	$L1_0$	−104	
AuPd	$L1_1$	−88	
AuPd	Nr 40	−118	
AuPd	V2	−37	
AuPd	Y2	−88	
AuPd	Z2	−66	
AuPd	D4	−80	
AuPd	SQS8	−79	

TABLE III. Enthalpies of formation in meV/atom for fully relaxed fcc-based structures in the Ag-Pt system as computed with the projector augmented planewave method.

Compound	Structure	ΔH_f	ΔH_f
Ag, Pt	A1	0	0
Ag_8Pt, $AgPt_8$	$NbNi_8$	1.6	15.4
Ag_7Pt, $AgPt_7$	Ca_7Ge	0.7	0.9
Ag_5Pt, $AgPt_5$	A_5B, C2/m	−1.5	24.3
Ag_4Pt, $AgPt_4$	$MoNi_4$	2.1	31.2
Ag_3Pt, $AgPt_3$	$L1_2$	26.6	39.5
Ag_3Pt, $AgPt_3$	$D0_{22}$	31.9	48.2
Ag_3Pt, $AgPt_3$	$L1_1^+$	5.5	6.7
Ag_3Pt, $AgPt_3$	V1	−4.3	−3.0
Ag_3Pt, $AgPt_3$	Y1	19.8	30.7
Ag_3Pt, $AgPt_3$	Z1	−5.3	21.2
Ag_3Pt, $AgPt_3$	SQS8	23.5	32.6
Ag_5Pt_2, Ag_2Pt_5	Mn_2Au_5	23.9	35.3
Ag_2Pt, $AgPt_2$	$MoPt_2$	18.4	13.3
Ag_2Pt, $AgPt_2$	CdI_2	−22.1	−6.0
Ag_2Pt, $AgPt_2$	A_2B, C2/m	11.4	11.6
AgPt	$L1_0$	63.2	
AgPt	$L1_1$	−39.3	
AgPt	Nr 40	65.5	
AgPt	V2	2.4	
AgPt	Y2	22.6	
AgPt	Z2	−5.1	
AgPt	D4	−27.3	
AgPt	SQS8	31.5	

value of -82 ± 20 meV/atom for the enthalpy of formation of Au_3Pd at 298 K. Our calculated values at $T=0$ K are −101 meV/atom for the $D0_{22}$ structure and −82 meV/atom for the SQS. Meschel and Kleppa[74] pointed out that it was impossible to perform x-ray diffraction analysis on the reacted sample, the electron microprobe technique used was not able to show conclusively if the sample was an ordered compound. This could explain why the value obtained by Meschel and Kleppa[74] is slightly less exothermic than our calculated value for the $D0_{22}$ structure and very similar to the value obtained for the SQS.

In the Au-Pd system, Weinberger *et al.*[37] observed strong variations of the pair interactions with the lattice parameter. In order to check this point, the total energies of the $L1_0$, 40, and $L1_1$ structures are reported as function of the volume in Fig. 4. Our results indicate some volume effects also because at small atomic volume the total energies of the $L1_0$, and Nr. 40 structures become identical while the $L1_1$ structure remains less stable than the two others structures. This agrees roughly with the trend in Fig. 6 of Ref. 37, where the $L1_1$ is clearly much less stable than $L1_0$ and Nr. 40, and where Nr. 40 is favored over $L1_0$ as the atomic volume increases. However, we do not see a switch from $L1_0$ to Nr. 40 in Fig. 4 although we consider up to 5% compression and extension of the equilibrium lattice parameter. In Fig. 1 of Ref. 38 it is apparent, however, that the $l_{max}=2$ approximation used in Ref. 37 has a significant influence of the lattice parameter prediction.

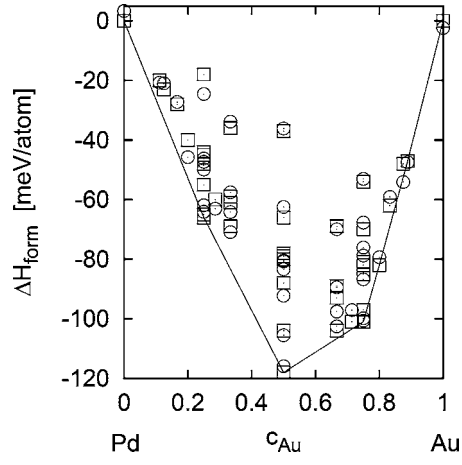

FIG. 3. Formation enthalpies of ordered structures in the Au-Pd system. Squares: DFT energies; circles: Energies as computed with the *R3M6N23* CE as described in the text. The thin solid line indicates the convex hull formed by the DFT ground state structures.

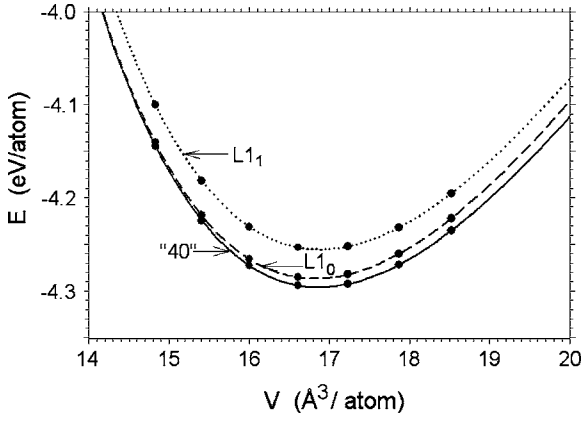

FIG. 4. Total energies of the $L1_0$, Nr 40, and $L1_1$ structures in the Au-Pd system as function of volume per atom.

Formation enthalpies of Ag-Pt alloys are shown in Fig. 5. The convex hull shows that only a single intermetallic groundstate is predicted: At equiatomic composition with the $L1_1$ structure. On the Ag-rich side, the CdI_2-type structure for the composition Ag_2Pt appears not so far from the straight line connecting fcc Ag and AgPt, $L1_1$. These two structures, $L1_1$ and α, are superlattices along the direction [111]. Other structures which belong to this family have formation enthalpies near zero. It is also interesting to note that the AB (D4) structure has a negative formation energy which is close to that of $L1_1$. Finel[75] has shown that the pair correlation functions in $L1_1$ and AB (D4) structures are the same and that the energy difference between the two structures is due mostly to the regular tetrahedron effective interaction whose value is usually small. All other studied structures have clearly positive enthalpies of formation. The SQSs enthalpies of formation are also positive and they display a slight asymmetrical shape with respect to 0.5 composition, with more positive values occurring at the Pt-rich side.

In Fig. 6 the simulated the x-ray diffraction spectrum of the relaxed $L1_1$ structure is shown. It compares well with the

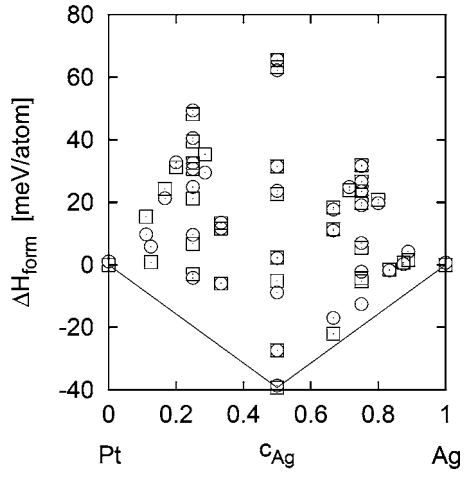

FIG. 5. Formation enthalpies of ordered structures in the Ag-Pt system. Squares: DFT energies; circles: Energies as computed with the *R*3*M*5*N*29 CE as described in the text. The thin solid line indicates the convex hull formed by the DFT ground state structures.

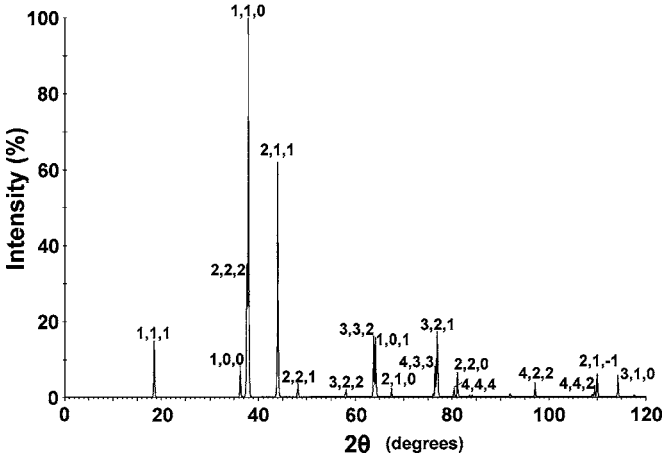

FIG. 6. Simulated x-ray diffraction pattern of the calculated fully relaxed $L1_1$ structure using Cu $K\alpha$ radiation (wavelength of 0.154 18 nm).

diffractogram presented by Durussel and Feschott[10] (Fig. 3 in that paper). In the absence of a single crystal these authors could not determine the exact structure of the $Ag_{15}Pt_{17}$ phase but they could determine that the structure was deformed cubic with 32 atoms in the cell. It is known that the $L1_1$ structure can be described in this way[76] also. Calculating the formation enthalpy of this supercell allowing relaxations gives the same value per atom as was obtained with the rhombohedral cell (see Table I). Our *ab initio* results confirm also the absence of any ordered $L1_2$ structure for the Ag_3Pt phase. Experimentally also, Erni *et al.*[12] did not find such an intermetallic.

In both Au-Pd and Ag-Pt systems, the lattice parameters of the various fcc superstructures are almost linear with composition. Such behavior is often observed in alloys where a single underlying lattice can be recognized and where ordering or phase separating tendencies are not very strong.

IV. CLUSTER EXPANSION

Substitutional alloys, such as Au-Pd and Ag-Pt, can exhibit an enormous number of possible ordered configurations. While the number of well-known fcc superstructures is limited to a few dozen structures, it is now well-recognized that there are many instances where uncommon structures occur.[36,73,77–79] Therefore, by performing density functional calculations for a few "usual suspect" structures one cannot be certain of the true ground states of an alloy system, no matter how accurate those calculations are. A case in point is the Ag-Pt alloy where, if one innocently omitted the rather uncommon $L1_1$ structure one would reach completely incorrect notions about the ground states. To aid in the search of the truly myriad possible ground states, CEs of the enthalpy have proved to be a powerful tool.[78,80–82] The aim is to simplify the electronic density functional Hamiltonian by mapping it onto a three-dimensional Ising-like Hamiltonian which has as degrees of freedom only the occupation of sites in the crystal. This is achieved by expanding the enthalpy in terms of composition-independent effective cluster interactions (ECIs),

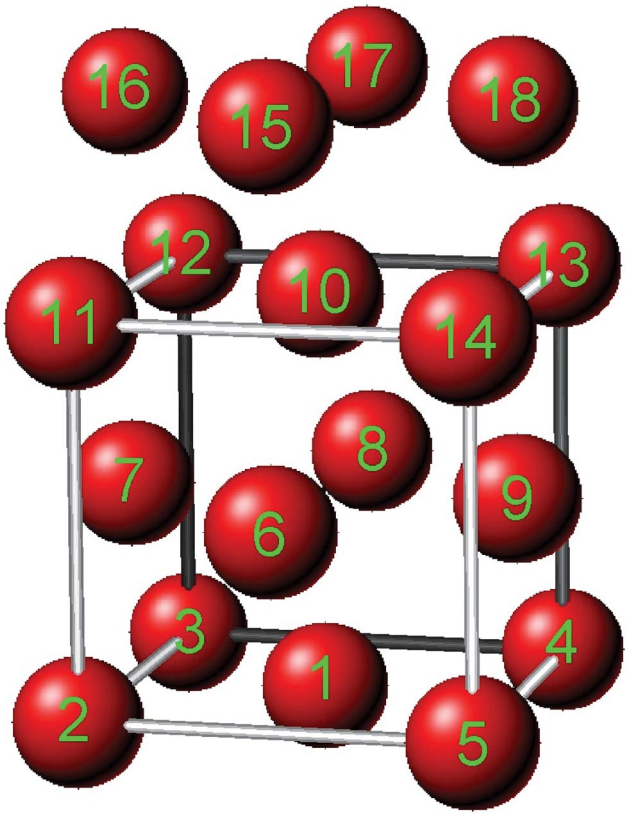

FIG. 7. (Color online) The three maximal clusters comprising the $R3$ approximation in relation to the fcc cube: First cluster consists of sites 1,3,4,6,7,8,9,10; second cluster sites 7,10,12,13,15,16,17; third cluster sites 6,7,10,12,13,15,16.

$$\Delta H_f^\alpha = \sum_i V_i \xi_i^\alpha, \tag{2}$$

where ΔH_f^α is the formation enthalpy of the α superstructure, ξ_i^α is the correlation function of cluster i in this superstructure as defined in Ref. 48, V_i is the ECI with its multiplicity on the fcc lattice folded in. Equation (2) is formally exact provided that the sum over i is extended over arbitrarily large clusters. However, for this expansion to be of practical use it must be truncated to a few terms only. Intuitively such a truncation is reasonable because chemical interactions have a dominant nearest neighbor pair character with minor corrections for angular distortions and also because the energy density associated with elastic defects in three dimensions decay as the sixth power of distance. When Eq. (2) is truncated it can be inverted so that formation enthalpies can be used to obtain the ECIs. Typically, the formation enthalpies of a large number of configurations are used to extract the ECIs following an extension of the Connolly and Williams[83] method (CWM), also known as the structure inversion method (SIM)[48] and the CE method.[81] Here, the ECIs are obtained by minimizing the fitting error

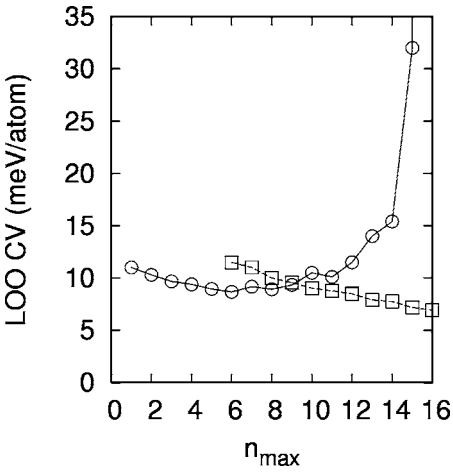

FIG. 8. Best leave-one-out cross validation scores (LOOCV) for invariant (circles) and noninvariant (squares) CE with clusters taken from the $R3$ set of clusters as computed by direct enumeration of all possible permutations in the case of Ag-Pt. n_{max} is the number of non-subclusters in the case of invariant CE, and it is equal to the total number of clusters in the case of noninvariant CE.

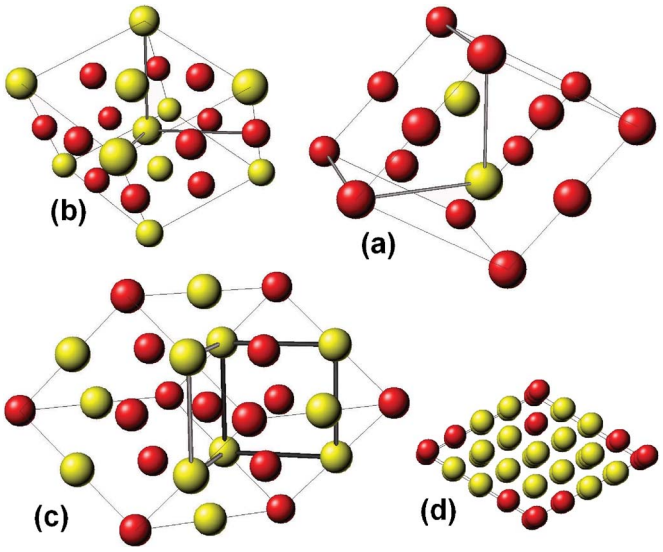

FIG. 9. (Color online) Structures predicted by CE: (a) Au_4Pd_2, (b) Au_5Pd_3, (c) Au_5Pd_3, and (d) $Ag_{12}Pt_4$. The Ag_4Pt_{12} structure is obtained from $Ag_{12}Pt_4$ by a reversal of Ag and Pt.

$$\sum_\alpha w_\alpha \left(\Delta H_f^\alpha - \sum_{i=0}^{n} V_i \xi_i^\alpha \right)^2, \tag{3}$$

where n represents the largest cluster included in the truncated summations and where optionally a weight[27,77,81,84–86] w_α can be assigned to structure α to impose that the correct low energy structures are reproduced by the ECIs when inserted back into Eq. (2). The weights also can greatly enhance the converge properties of the cluster expansion.[87] Here, no such weights were found necessary. *A priori*, it is not apparent which clusters should be included in the expansion beyond the first few near-neighbor pairs and the nearest-neighbor triangle. Our initial pool of clusters were all clusters in which no two sites are farther than the third nearest neighbor apart. For convenience we introduce the following nomenclature: Rn is the set of clusters which satisfy the condition that no two sites in a cluster are farther apart than the nth nearest neighbor. Among the $R3$ clusters there are three

clusters that are not contained in any other cluster in the set, other than themselves—these maximal clusters as they are called within the cluster variation formalism, we call the $R3$ maximal clusters, see Fig. 7. It is of interest to note that the commonly used tetrahedron and tetrahedron-octahedron (TO) maximal cluster approximations correspond to the largest clusters that can be formed with sites being not more than first nearest, or second nearest neighbor distances apart. The tetrahedron, and the TO maximal clusters thus are the $R1$ and $R2$ maximal clusters. Hence, the $R3$ is a natural extension beyond these approximations. The Rn maximal clusters were shown to be particularly advantageous in the context of the CVM.[48,88] The set of $R3$ subclusters includes 3 pairs, 7 triangles, 16 4-site, 17 5-site, 15 6-site, 6 7-site, and one 8-site clusters, as well as the empty and point clusters for a total of 67 clusters. As we used a set of 42(40) structures to extract ECIs for Au-Pd(Ag-Pt), without additional constraints[81] at most 42(40) ECIs can be extracted. Hence, a selection must be made from the 67 clusters in the initial set. Actually, we wish to have an overdetermined system of equations [Eq. (3)] in order to be able to verify the validity of the CE. The validity is evaluated with the predictive error[77] also known as the leave-one-out cross validation score (LOOCV).[78,89] Recently, it was shown that in order for a CE to be (1) defined uniquely in terms of the clusters included and to be 2) invariant with regard to the definition of the single site spin variable, all subclusters of included clusters must be included also.[49] This invariance criterion has been imposed also by other practitioners of clusters expansions.[89,90] For fitting purposes the cluster expansion does not need to satisfy the invariance or "include all sub-clusters criterion." But, in that case invariance with respect to the spin variable definition requires that there are "hidden" constraints: Namely the ECI associated with the clusters needed to make the CE complete are implicitly set to zero. When the definition of the site occupation variable is changed, say reversed, then these implicitly zero-valued ECIs generally take nonzero values.[49]

An invariant cluster expansion can be characterized in terms of its largest clusters,[49] for convenience here called "non-subclusters." A systematic method for finding the best invariant CE can be formulated. One starts by allowing only a single non-subcluster, then without regard for the earlier result, one considers all possible cases with two non-subclusters, and so forth until a certain maximum number of non-subclusters n_{max} has been evaluated. Here, we considered all possible invariant CE that can be formed with clusters from the $R3$ set. There are 4 677 954 possible invariant CE that can be formed from the $R3$ set of clusters if one allows not more than 40 ECIs in the CE. When additionally one ignores all ECIs associated with clusters with 6 and more sites, this number reduces to 2 180 526 with a greatest number of non-subclusters of 16. For each number of non-subclusters one considers the CE which minimizes the LOOCV. Of course, the total number of clusters in an invariant CE is considerably larger than the number of non-subclusters in that CE: The invariant CE with the lowest LOOCV for $n_{max}=2\cdots7$ have each in total about 20 clusters, while for $n_{max}=8\cdots12$ there are about 30 clusters in the CE. Unlike the fitting error, i.e., the root mean square difference of CE and DFT enthalpies, the predictive error does not monotonically decrease as more and more non-subclusters are added, as is illustrated in Fig. 8. It is evident that for invariant CEs, once there are more than about 6 non-subclusters, adding more non-subclusters no longer improves LOOCV scores. One reason is that with too many non-subclusters the system of equations becomes underdetermined, meaning too many ECIs need to be determined from too few structural energies. Also, the $R3$ set of clusters has only a limited number of "small" clusters, so that very quickly because of the restraints of the $R3$ set one must include many-body clusters which are known to be energetically less relevant.

Noninvariant CEs are still very far from underdetermined at the practical enumeration limit of about 16 clusters in the CE, see Fig. 8. However, for noninvariant CEs also, eventually underdeterminedness comes into play so that an optimal number of clusters in the CE exists. In the case of noninvariant CE this optimal number is so large and requires so many evaluations that it can be found only through approaches such as simulated annealing or genetic algorithms.[78,82] Here, we will consider invariant CEs only.

As was discussed recently by Blum and Zunger,[78] the predictive error (LOOCV) alone is not a completely satisfactory criterion for selecting the best CE. One reason is that the set of clusters in the CE is selected on the basis of the structures for which energies are available, so that when one "leaves one structure out" there is still some information relating to this structure present in the way that the CE has been selected. To overcome that shortcoming, we added 3 (2) structures in the case of Au-Pd (Ag-Pt) and checked how well these structures were truly predicted by the invariant CEs. Details of these structures are given in Fig. 9. It should be remarked, that here the direct enumeration method is particularly convenient, as one can simply keep a pool of the best invariant CEs, and then select from among this pool with additional criteria, such as predicting unknown structures. Table IV shows that the CE with the best LOOCV error does not give the best prediction for the new structures. The invariance criterion severely limits the number of allowable CE, making possible the direct enumeration method, but another strength is that it disfavors large clusters in the CE because the many subclusters quickly lead to overfitting and deterioration of the predictive error. Thus, to some extent it is a protection against a shortcoming of the predictive error (leave-one-out cross-validation score)[91] as optimizing criterion.

The cluster variation method[48,50–52] requires small, compact clusters for a good description[48,88] of the configurational entropy. The internal energy, on the other hand, does not have such a requirement and in fact there are many studies in which very long-ranged effective pair interactions are shown to be essential to describe subtle structural effects and short range order.[25,31,33] Nevertheless, there are many alloys in which the only known superstructures can be stabilized by short-ranged ECI and there are also many successful phase diagram calculations with short ranged ECIs.[14,18,26,77,84,85,89,92–97] To evaluate how a CE with many many-site clusters performs in comparison with a CE with mainly pair ECIs, we considered also CEs formed from the

TABLE IV. Comparison of CEs in terms of fitting error (root mean square), leave-one-out cross validation (LOO CV), and prediction of 3 favorable structures suggested by a ground state search. Also listed are non-subclusters and total number of clusters in the CE. DFT refers to fully relativistic density functional calculations. $R2 \cup R10S2$ is the union of $R2$ and $R10S2$, where $S2$ refers to the limitation of at most 2 sites, so that $R10S2$ refers to the 10 nearest neighbor pairs and the point cluster. M refers to the number of non-subclusters in the CE, while N indicates the total number of clusters in the CE. All energies in meV/atom.

		Au-Pd			
			extra str.		
CE	Fit error	LOO CV	(a) Au_4Pd_2	(b) Au_5Pd_3	(c) Au_5Pd_3
DFT	—	—	−110.4	−110.6	−109.9
R3 M8 N32	1.5	4.8	−117.7	−118.3	−133.5
R3 M6 N23	3.5	9.6	−109.7	−111.5	−111.8
R2∪R10S2 M10 N19	5.9	11.8	−102.5	−106.3	−105.8
R2∪R10S2 M7 N12	6.3	9.4	−99.5	−102.7	−100.5
R2 M2 N11	6.9	10.2	−104.8	−104.8	−104.8
		Ag-Pt			
				extra str.	
CE	Fit error		LOO CV	(d) $Ag_{12}Pt_4$	(d) Ag_4Pt_{12}
DFT	—		—	−21.7	20.2
R3 M6 N21	4.8		8.6	−2.7	−8.7
R3 M5 N29	2.6		8.7	−23.2	−19.7
R2∪R10S2 M10 N19	4.6		8.8	6.8	19.7
R2∪R10S2 M6 N15	5.5		7.9	7.7	19.8
R2 M2 N11	8.5		12.2	−6.7	5.2

set of clusters provided by the first 10 nearest-neighbor pairs and the clusters contained within the tetrahedron-octahedron clusters, indicated by $R2 \cup R10S2$, where the "S" refers to the number of sites. This second pool of clusters has only 19 members (10 pairs, 2 triangles, 3 4-site, 1 5-site, and 1 6 site clusters, as well as the empty and point clusters) which is many fewer than the $R3$ set. In spite of the smaller number of clusters in the set $R2 \cup R10S2$ than in the set $R3$, Table IV shows that it gives CEs that give similar fitting errors, LOOCV and structural energy predictions as the CEs from the $R3$ set, while the latter typically involve a larger number of ECIs (the number following N in Table IV). This agrees with the results of Zunger and co-workers,[25,33,47,78,79,82,98] and agrees also with predictions of the generalized perturbation method—coherent perturbation method.[60,93,99,100]

Use of the CVM biases us to use the CE derived from the $R3$ set because this CE can be easily used within the $R3$ cluster approximation. While there are some approximate methods available to include long-ranged pair interactions within the CVM,[101] these are generally cumbersome and not particularly accurate from a statistical mechanical point of view. For Au-Pd we selected the $R3M6N23$ CE over the $R3M8N32$ CE because the former gave a better agreement with the convex hull from DFT. The fact that the LOOCV for the $R3M8N32$ CE is better by about 5 meV/atom we judged to be much less significant in view of the errors inherent in any DFT calculations and in view of the limitations of our current approach where vibrational effects were completely neglected. The $R3M6N23$ CE contains the six non-subclusters which can be recognized in Fig. 7 as given by the sites: First cluster 7,11,12,16; second cluster 1,4,7,10; third cluster 1,3,4,10; fourth cluster 1,3,4,7,8; fifth cluster 1,3,4,7,9; sixth cluster 6,12,13,15,16. Of course, in addition to these six clusters there are another 17 clusters that are subclusters. This expansion reproduces the enthalpies of formation very well as is apparent from Table IV and Fig. 3. However, some limitations of the quality of the fit are apparent: $NbNi_8$-type Au_8Pd is not a ground state according to the CE, it has been replaced incorrectly by the Ca_7Ge-type Au_7Pd structure, the Ni_4Mo-type Au_4Pd is omitted as a ground state, and for Au_3Pd the enthalpy difference between $L1_2$ and $D0_{22}$ is quite a bit larger in the DFT results than in the CE.

For Ag-Pt the $R3M5N29$ CE was selected over the $R3M6N21$ CE for similar reasons as in the case of Au-Pd, but here the difference in LOOCV scores is truly negligible. The $R3M5N29$ CE has five non-subclusters, given by the sites: First cluster 6,7,10,11; second cluster 8,10,12,16; third cluster 1,3,4,6,8; fourth cluster 6,10,12,13,15; fifth cluster 6,7,10,13,15,16. While these two CEs for Au-Pd and Ag-Pt involve different non-subclusters it should be borne in mind that most subclusters are the same, such as the pair and tri-

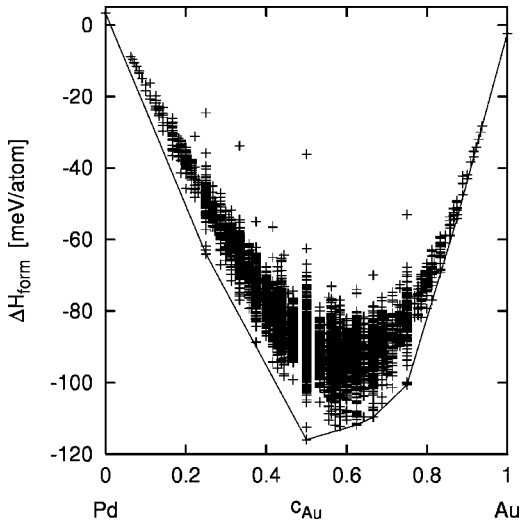

FIG. 10. Formation enthalpies of all structures with translation vectors of length less or equal to the sixth nearest neighbor $\langle(111)\rangle$ as computed with Eq. (2) using the ECIs from the $R3M6N23$ CE for Au-Pd. The vertices at compositions Au_2Pd and Au_5Pd_3 represent the prospective ground-state structures shown in Figs. 9(a)–9(c). Note that at Au_5Pd_3 there are two energetically almost degenerate structures.

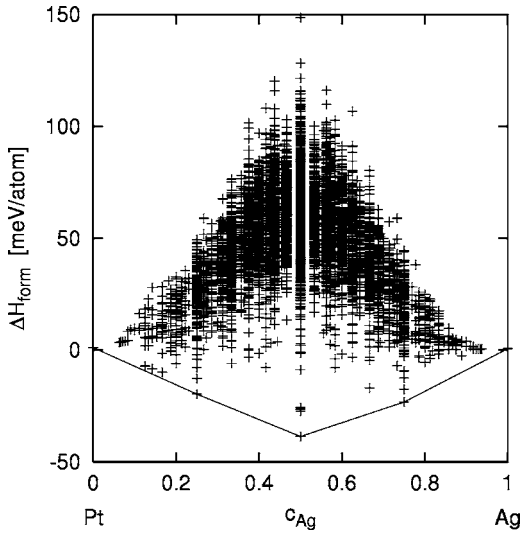

FIG. 11. Formation enthalpies of all structures with translation vectors of length less or equal to the sixth nearest neighbor $\langle(111)\rangle$ as computed with Eq. (2) using the ECIs from the $R3M5N29$ CE for Ag-Pt. The vertices at compositions Ag_3Pt and $AgPt_3$ represent the prospective ground-state structures shown in Fig. 9(d).

angle subclusters. The $R3M5N29$ CE represents the DFT enthalpies very well also, for some structures, such as the SQS structures, the CE gives almost identical values as the DFT.

A. Ground state search

A much more critical test for a CE is whether it can predict ground states that were not considered in the DFT calculations. In other words, the CE is used to search for new possible ordered states.[78,82,98] Here, we generated all structures with primitive translation vectors corresponding to pairs up to and including the sixth nearest neighbor (the fcc cube body diagonal). This gave rise to 6214 unique structures and we used Eq. (2) with the CEs obtained for Au-Pd and Ag-Pt to compute the formation enthalpy of each structure. The results of these computations are displayed in Figs. 10 and 11.

In Au-Pd the most salient feature is how little the convex hull has changed by considering more than 6000 additional structures. Nr. 40, the structure with the largest formation enthalpy, is still the most stable; the other $\langle 1\frac{1}{2}0\rangle$ structures also, Au_3Pd and $AuPd_3$ with the D022 structure remain ground states; Ca_7Ge-type Au_7Pd structure still is an incorrect, but only very marginally stable, ground state. The most interesting features occur between Au concentrations 0.6 and 0.7 and near Au concentrations 0.9. At these compositions there are many structures very close to the ground state line and in fact two new ground states are predicted: Au_4Pd_2 [Fig. 9(a)] and Au_5Pd_3 [Fig. 9(c)] with another structure [Fig. 9(b)] energetically almost degenerate. It is quite likely, that if structures with even longer translation vectors had been considered other ground states would have been found that would have lowered the convex hull a tiny bit more. The presence of many, energetically almost degenerate structures in these composition ranges is probably much more significant than finding a particular lowest energy structure. The DFT formation enthalpies have been calculated (see Table IV) and only Au_4Pd_2 [Fig. 9(a)] is then found to lie on the convex hull, although the other two Au_5Pd_3 structures are found to be within about 2 meV/atom from the hull. The stability of the two Au_5Pd_3 structures is reversed, but this is not surprising considering the very small energy differences involved.

In Ag-Pt the convex hull has changed a bit more by considering an additional 6000 structures: Two new ground states are found, at Ag_3Pt and at $AgPt_3$. Surprisingly, these structures are the same [Fig. 9(d)], but in contrast to Ag_3Pt, $AgPt_3$ is predicted to be only marginally stable. Actual DFT calculations confirm reveal that Ag_3Pt is a ground state. However, the prediction for $AgPt_3$ is completely wrong—it is not even close to being a ground state (see Table IV). In Fig. 5 it is apparent also, that while for many structures the CE is very close to the DFT enthalpies, for other structures the agreement is much poorer. It is not likely that the Ag_3Pt structure can be formed in actual alloys because its enthalpy is only just below the average of that of the Ag-fcc and the AgPt $L1_1$ structures, meaning that the driving force for the formation of Ag_3Pt is of the order of 2 meV/atom only.

B. Mixing enthalpy and SQS

The mixing enthalpy, actually the formation enthalpy of the configurationally random solid solution, can be obtained from the CE also using the relation

$$\Delta H_{mix} = \Delta H_f^{random} = \sum_{i=0} V_i \xi_1^{N_i}, \tag{4}$$

where the superscript *random* refers to the configurationally random substitutional alloy, ξ_1 is the point correlation func-

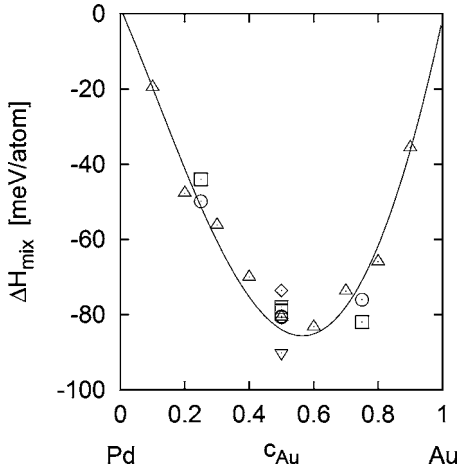

FIG. 12. Mixing enthalpies: As computed with Eq. (4) using the ECIs from the *R*3*M*6*N*23 CE for Au-Pd (solid line); as obtained from DFT calculations on SQS (squares); as computed with Eq. (2) for SQS (circles); calorimetry from Ref. 42 (triangles pointing up); calorimetry from Ref. 103 (diamond); calorimetry from Ref. 104 (triangle pointing down).

tion and N_i is the number of sites in cluster i. The mixing enthalpies of Au-Pd and Ag-Pt alloys are displayed in Figs. 12 and 13.

In the case of Au-Pd the results from the CE together with Eq. (4) can be compared with values from SQS and can be compared also with calorimetric data from experiment[42,43,103,104] (see also Fig. 12). The CE predicts a mixing enthalpy that compares quite well with that obtained from DFT calculations on SQS: The correct asymmetry with respect to composition is seen. The SQS formation enthalpies as obtained from the CE with Eq. (2) are in even better agreement with the CE mixing enthalpy. As the SQS are designed to reproduce the correlation functions of the random configuration especially for pairs and for compact triangles, this shows that in the CE ECIs associated with many-site clusters are not so important for the enthalpy. The CE mixing enthalpy agrees very well with the data by Darby[42] as reported in Ref. 102 and Hayes and Kubaschewski.[43] Darby[42] measured the mixing enthalpy of several Au-Pd alloys using tin solution calorimetry. In these measurements, the samples were introduced in the calorimeter from room temperature. However, considering the sample preparation with a final heat treatment at 1173 K for 2 h followed by water quenching, one may assume that the alloys are in a disordered state with a short range order corresponding to 1173 K. Considering that ordering tendencies in Au-Pd are rather weak—the highest order-disorder system is predicted to be under 500 K as will be shown below—a temperature of 1173 K should be sufficient to effectively eliminate short range order in the solid solution. Hayes and Kubaschewski[43] determined the enthalpy of formation of some alloys by direct reaction calorimetry at 300 °C. The experimental data from Darby[42] and Hayes and Kubaschewski[43] agree well with each other. Indirect measurements of the mixing enthalpy of the disordered Au-Pd solid solution have been performed by Höhn and Herzig[103] and by Tomiska.[104] For 0.5 composition, Höhn and Herzig[103] obtained a value of the enthalpy of mixing of −74 meV/atom at 1200 K which is in good agreement with the value of Darby.[42] Tomiska[104] got slightly more negative values of the enthalpy of mixing: −90 meV/atom at 1500 K for equiatomic composition. Our calculated values, both from the CE and from the DFT calculation on SQS, are right between these two experimental values.

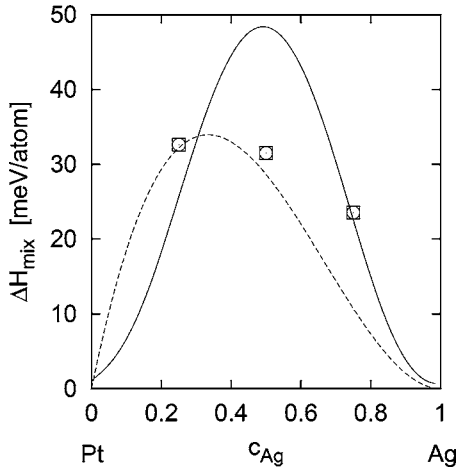

FIG. 13. Mixing enthalpies: As computed with Eq. (4) using the ECIs from the *R*3*M*5*N*29 CE for Ag-Pt (solid line); as obtained from DFT calculations on SQS (squares); as computed with Eq. (2) for SQS (circles); as extracted from Ref. 8 by extrapolation to a temperature of 0 K (dashed line).

In the case of Ag-Pt we could not find experimental data pertaining to the mixing enthalpy. The Gibbs energy as function of composition and temperature was obtained by Ebert *et al.*[8] by fitting to the experimental phase diagram. By extrapolating the excess Gibbs energy down to a temperature of 0 K, which is far outside the temperature range for which the Gibbs energy was determined, and hence is a rather questionable procedure, and by using Eq. (2) with the parameters in Table 1 from Ref. 8, the dashed curve in Fig. 13 was obtained. Although this procedure often gives less than reliable mixing enthalpies,[105] here it gives about the right the magnitude, and the asymmetry with respect to equiatomic composition mirrors that seen in the SQS emthalpies, although the CE mixing enthalpy lacks this asymmetry. Surprisingly, while the DFT formation enthalpies of the SQS are very well described by the CE, the mixing enthalpy as computed by the CE is quite far from the SQS enthalpies (see also Fig. 13). The reason that the CE mixing enthalpy differs noticeably from the SQS enthalpies may point to a limitation of the *R*3 set of clusters: If long-ranged (pair) interactions play an important role, then a set of clusters that includes only the three nearest neighbor pairs might project the contributions of those distant pairs on to many-site clusters. This implies that a short-ranged CE may exaggerate the energy contributions from ECIs associated with many-site clusters. Since at equiatomic composition, the ECIs associated with odd numbers of sites do not contribute to the mixing enthalpy if Ising type occupation numbers are selected,[49] the large difference between the CE mixing enthalpy and the SQS enthalpy at equiatomic composition suggests that especially the 4-site clusters might be exaggerated in the *R*3*M*5*N*29 CE for Ag-Pt.

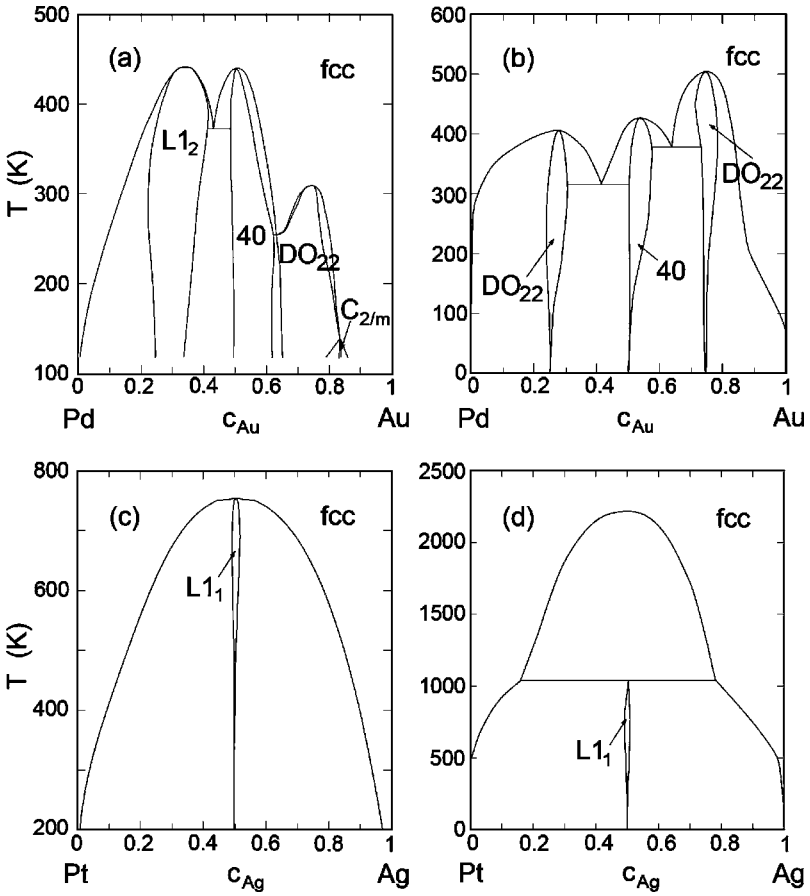

FIG. 14. Phase diagrams computed with the CVM: (a) Au-Pd using the *R*2 CE in the *R*2 (TO) approximation of the CVM, (b) Au-Pd using the *R*3*M*6*N*23 CE with *R*3-CVM, (c) Ag-Pt using the *R*2 CE with *R*2-CVM, (d) Ag-Pt using the *R*3*M*5*N*29 CE with *R*3-CVM.

Other reasons to suspect that the highly symmetric CE mixing enthalpy might be incorrect are (a) the asymmetrical shape of the two-phase region between the fcc solid solutions in the various phase diagrams in the literature[4–10] (although admittedly effects not considered here, such as vibrational entropy could play a role[106–108]) and (b) the not-so symmetrical distribution of formation enthalpies in Fig. 5.

V. Au-Pd AND Ag-Pt PHASE DIAGRAM CALCULATIONS

Phase diagrams have been calculated using the CVM considering configurational effects only. No attempt was made to include vibrational effects. Now, two approximations must be kept in mind: (1) The maximal clusters used to obtain the CE, and (2) the maximal clusters used in the CVM. The maximal clusters used in the CVM should be as large, or larger, than the maximal clusters used in the CE because otherwise there will be ECIs that cannot be used in the CVM energy expression.[101]

First we examined if the *R*3 CVM gave similar results as the *R*2 CVM while using the same CE. The *R*2 CVM, better known as the tetrahedron-octahedron approximation of the CVM, handles only 11 clusters (empty cluster, point, 2 pairs, 2 triangles, 3 four-site, pyramid, and octahedron) and given that 40 (Ag-Pt) or more (Au-Pd) structures are to be represented we decided to use all clusters for the CE (*R*2 CE). Of course, because the *R*2 CE has 11 terms only it does not yield a very good fit (see row *R*2*M*2*N*11 in Table IV) and many ground states are wrong. The phase diagrams calculated with the *R*2 CE using the *R*2 CVM and the *R*3 CVM were almost the same for both Au-Pd and Ag-Pt: Critical temperatures differed of the order of 1%, therefore we show only the *R*2 CVM results for the *R*2 CE in Figs. 14(a) and 14(c). That the *R*2 and *R*3 CVM give almost identical results indicates that from a statistical thermodynamics view point the *R*2 CVM is already accurate enough for a description of the configurational entropy. The same cannot be said about the configurational energy, however.

In Figs. 14(a) and 14(b) the Au-Pd phase diagram is shown as computed with the *R*2 CE and as computed with *R*3*M*6*N*23 CE. While there are important similarities: The temperature scale, the ordered compounds at Au_3Pd, AuPd, and $AuPd_3$, and for the first two even the specific structures, there are also some important differences. The *R*2 CE finds different ground states, there is no ground state at Au_5Pd with the $C_{2/m}$ structure and at $AuPd_3$ there is a ground state, but of the DO_{22} type rather than of the $L1_2$ type. On these counts the *R*3*M*6*N*23 CE performs better, giving ground states that generally agree with the DFT calculations, although marginally stable ground states are still incorrect as was mentioned earlier. Figure 14(b) does not agree so well with the assessment by Okamoto and Massalski[2,3] (redrawn in Fig. 1), but it must be emphasized that experimental data is scarce. Two compounds have been reported without structural details: Au_3Pd with a transition to the disordered fcc solid solution at $T_c=1133$ K[109] and $AuPd_3$ with $T_c=1043$ K[110] or $T_c=1148$ K.[111] For AuPd no compound has been reported, after annealing at 923 K and cooling to room

temperature Maeland and Flanagan[112] found an fcc solid solution by x-ray diffraction. Iveronovna and Katsnelson[113] estimated an order-disorder temperature $T_c = 100\ ^\circ C$, which is rather close to the 150 °C shown in Fig. 14(b), based on short range order parameter measurements at 400 and 600 °C. Okamoto and Massalski adopted this order-disorder temperature of 100 °C in their assessment.[2,3] Computer simulations of the short range order have pointed to long-period superlattices for AuPd.[114] In our cluster expansions the effective interactions are limited to the third nearest neighbor, so that we are not capable of describing such long-period superlattices, but comparing just the energies of $L1_2$ and DO_{22} at the compositions Au_3Pd and $AuPd_3$ indicates that the energy difference is very small: Only 0.1 eV/atom for $AuPd_3$ (see Table II). Such small energy differences are known from other systems[60] and strongly suggest that long-period superlattices might occur in the Au-Pd phase diagram, and then particularly so at the Pd-rich side. For Au_3Pd and $AuPd_3$ we appear to have much lower order-disorder temperatures than experiment, see Fig. 1. To the best of the authors' knowledge there are no other fcc-based phase diagrams with two ordered A_3B and AB_3 structures with T_c's more than twice as high as the T_c of an intermediate AB structure, so that the assessed phase diagram (Fig. 1) appears improbable. The predicted diagrams, Figs. 14(a) and 14(b) appear more "plausible" in this regard. As mentioned, the very small energy differences between $L1_2$ and DO_{22} structures suggests long-period superlattices which we cannot describe with our CE, or with our $R3$-approximation of the CVM. It is of some interest to point out that the difference in T_c for the Au_3Pd phase is increased by a factor of almost two when we go from the $R2$ to the $R3M6N23$ CE. However, we attribute this change mostly on the rather poor fit to the formation enthalpies in the $R2$ CE. Given that the energy differences between the various long-period superlattices are small, that the $R3M6N23$ CE gives a rather close fit to the formation enthalpies, and given that the $R3M6N23$ CE gives a reasonable estimate for the T_c of AuPd, we do not expect that even if we extended the range of the interactions in the CE the T_c would reach the 1100 K as reported experimentally.[109–111] Only detailed experimental studies will lay these speculations to rest.

In Figs. 14(c) and 14(d) the Ag-Pt phase diagram is shown as computed with the $R2$ CE and as computed with $R3M5N29$ CE. Both the $R2$ and $R3M5N29$ CE indicate that $L1_1$ AgPt is the only compound in the Ag-Pt system. Agreement exists even as to the highest temperature this phase can exist, in both cases of the order of 1000 K. However, the $R2$ CE does not produce a miscibility gap at elevated temperatures. Many attempts were made to coax this feature out of the $R2$ CE by selectively omitting structures from the structural inversion, and by selectively omitting clusters from the $R2$ CE. None of these produced a miscibility gap in the fcc solid solution above the AgPt phase. The high-temperature miscibility gap is a feature that apparently requires a more extended set of clusters than available in the $R2$ CE. The clusters in the $R3M5N29$ CE give a miscibility gap, but it should be mentioned that there are other $R3$-based CE, with poorer LOOCV, that give phase diagrams more similar to the $R2$ CE results. The $R3M5N29$ CE phase diagram agrees on several points with a recent experimental phase diagram by Durussel and Feschotte[10] (see Fig. 2): The AgPt $L1_1$ is the only compound with a narrow range of composition, it decomposes through a peritectoid reaction at about 1000 K (in good agreement with the experimental value of 1076 K[10]), a miscibility gap with a critical temperature of 2200 K (to be compared with about 2000 K extrapolated in Fig. 2). The predicted phase diagram [Fig. 14(d)] deviates in one aspect only quantitatively from the Durussel and Feschotte phase diagram[10] (Fig. 2): Experimentally the solubility of Pt in Ag is considerably greater than the solubility of Ag in Pt, while the calculated phase diagram is rather symmetrical. Notwithstanding the excellent agreement between the predicted phase diagram [Fig. 14(d)] and the experimental phase diagram by Durussel and Feschotte[10] and also that by Johansson and Linde[5] from 1930, there are many other experimental reports that to a greater or lesser degree disagree. The oldest reported phase diagram,[4] by Doerinckel, agrees in many aspects but does not give any compound. The diagram by Schneider and Esch[6] disagrees on almost every point: We do not confirm a compound Ag_3Pt with the $L1_2$ structure and transformation temperatures of 960 and 782 °C, and we also do not find an $AgPt_3$ compound with transformation temperatures of 698 and 619 °C. Klement and Luo[7] also report an Ag_3Pt compound with a T_c of 965 °C. Ebert *et al.*[8] present a phase diagram with somewhat similar phase boundaries for the fcc solid solutions, but without any AgPt compound. Finally, the assessed phase diagram of Karakaya and Thompson[9,11] displays compounds at Ag_3Pt and $AgPt_3$ with transition temperatures as reported earlier.[6,7] It should be mentioned that Erni *et al.*[12] concluded that the phase Ag_3Pt with $L1_2$ structure does not exist through transmission electron microscopy analysis of $Ag_{85}Pt_{15}$. It is apparent that while the literature on Ag-Pt is highly contradictory, our theoretical phase diagram strongly supports the Johansson and Linde[5] and the Durussel and Feschotte[10] versions of the Ag-Pt phase diagram.

It has become apparent that the Au-Pd and Ag-Pt systems are profoundly different in spite of the similarity in the electronegativity and atomic volume differences in both systems. Spin-orbit effects were seen to play a very minor role, a few meV/atom at most, which represent a small fraction of the formation and mixing enthalpies only. While the mixing enthalpy in Au-Pd is negative, it is positive in Ag-Pt. Moreover, the mixing enthalpy in Au-Pd is rather symmetric with respect to equiatomic composition, but it appears asymmetric in the Ag-Pt case (see Fig. 13). The reason for this is most likely found in the strain energy part of the mixing. While Au and Pd have fairly similar bulk moduli (173 and 193 GPa, respectively[115]), the bulk moduli for Ag and Pt are very dissimilar (104 and 283 GPa, respectively[115]). The strain energy is proportional to the bulk modulus, so that its variation with composition strongly affects the symmetry of the strain part of the mixing enthalpy. Hence, while the strain energy in Au-Pd is symmetric, in Ag-Pt the strain energy is small at the soft Ag-rich side, and is large at the hard Pt-rich side. It is thus not surprising that Ag does not dissolve as well in Pt, as that Pt dissolves in Ag, because the latter is more accommodating. It is very likely that these differences between Au-Pd and Ag-Pt in elastic behavior also are reflected in the inter-

atomic force constants and thus in the vibrational entropy. This suggests that bulk modulus differences are just as important an indicator for alloy behavior as atomic size differences.

VI. CONCLUSIONS

Over the past decades *ab initio* methods have proved accurate and useful tools for the prediction of ground states and thermodynamic properties. Especially in alloy systems where significant disagreement or uncertainties in the experimental data or assessments of this data exists, *ab initio* studies can offer valuable insights such as in the case for Au-Pd and Ag-Pt systems. At first glance these two alloys appear simple fcc-based systems with similar atomic size mismatch and similar electronic structures. Closer examination shows that while Au-Pd is clearly an ordering system with predominantly $\langle 1\frac{1}{2}0\rangle$ type ordering wave vectors and possibly with long-period superlattices, Ag-Pt exhibits ordering exclusively for structures with $\langle \frac{1}{2}\frac{1}{2}\frac{1}{2}\rangle$ type ordering wave vectors and probably in the immediate vicinity of equiatomic composition only, while at higher temperatures a miscibility gap exists in the fcc solid solution.

In the Au-Pd system compounds were found at the experimentally known compositions. Predicted enthalpies of formation agreed very well with those determined with calorimetry.[42,43,74,103,104] The UPb prototype[40] structure (Nr 40) is predicted the most stable phase for AuPd. Experimental proof for the existence of this structure is still lacking, probably due to the low order-disorder temperature. The order-disorder temperatures are found to be low, less than 200 °C, which agrees with experimental data for the equiatomic phase. However, it does not agree with the anomalously high order-disorder temperatures tentatively presented in the assessed phase diagram for Au_3Pd and $AuPd_3$ compounds,[2,3] see Fig. 1.

In the Ag-Pt system, the $L1_1$ structure is predicted as the only stable compound at ambient temperature, while at very low temperature there may be a marginally stable Ag_3Pt phase. The structure of the $Ag_{15}Pt_{17}$ compound detected by Durussel and Feschott[10] appears closely related to the $L1_1$ structure. The Ag_3Pt and $AgPt_3$ ordered structures with order-disorder temperatures of 1000 K and over which have appeared in Ag-Pt phase diagrams since the 1940s[6,7,9,11] are not confirmed in this work. Recent experimental work[10,12] suggests also that these phases do not exist. Only by using a cluster expansion with effective interactions beyond the second nearest neighbor shell was it possible to obtain an fcc phase diagram that agrees with the main features presented by the most authoritative experimental phase diagram.[10]

ACKNOWLEDGMENTS

One of the authors (M.S.) gratefully acknowledges support from the Netherlands Organization for Scientific Research (NWO) and the Netherlands Institute for Metals Research (NIMR) through a research program of the Foundation for Fundamental Research of Matter (FOM). The authors gratefully acknowledge PHYNUM at LPMMC for computational resources (A.P.).

*Electronic address: M.H.F.Sluiter@tudelft.nl

[1] T. B. Massalski, *Binary Alloy Phase Diagram*, 2nd ed. (ASM International, Materials Park, OH, 1990).
[2] H. Okamoto and T. B. Massalski, Bull. Alloy Phase Diagrams **6**, 229 (1985).
[3] H. Okamoto and T. B. Massalski, in *Binary Alloy Phase Diagrams*, 2nd ed., edited by T. B. Massalski (ASM International, Materials Park, Ohio, 1990), Vol. 1, pp. 409–410.
[4] F. Doerinckel, Z. Anorg. Chem. **54**, 333 (1907).
[5] C. H. Johansson and J. O. Linde, Ann. Phys. **6**, 458 (1930).
[6] A. Schneider and U. Esch, Z. Elektrochem. Angew. Phys. Chem. **49**, 72 (1943).
[7] W. Klement and H. L. Luo, Trans. Metall. Soc. AIME **227**, 1253 (1963).
[8] H. Ebert, J. Abart, and J. Voitlander, J. Less-Common Met. **91**, 89 (1983).
[9] I. Karakaya and W. T. Thompson, Bull. Alloy Phase Diagrams **8**, 334 (1987).
[10] Ph. Durussel and P. Feschotte, J. Alloys Compd. **239**, 226 (1996).
[11] I. Karakaya and W. T. Thompson, in *Binary Alloy Phase Diagrams*, 2nd ed., edited by T. B. Massalski (ASM International, Materials Park, Ohio, 1990), Vol. 1, pp. 77–79.
[12] R. Erni, T. Etter, H. Heinrich, and G. Kostorz, Z. Metallkd. **92**, 1194 (2001).
[13] S. Takizawa, K. Terakura, and T. Mohri, Phys. Rev. B **39**, 5792 (1989).
[14] T. Mohri, S. Takizawa, and K. Terakura, Mater. Trans., JIM **31**, 315 (1990).
[15] T. Mohri, K. Terakura, S. Takizawa, and J. M. Sanchez, Acta Metall. Mater. **39**, 493 (1991).
[16] T. Mohri, S. Takizawa, and K. Terakura, J. Phys.: Condens. Matter **5**, 1473 (1993).
[17] T. Mohri, I. Yamagishi, T. Suzuki, C.-S. Oh, D. N. Lee, M. Yashima, M. Yoshimura, and C. Ohno, Z. Angew. Math. Mech. **86**, 353 (1995).
[18] C. Colinet and A. Pasturel, Z. Angew. Math. Mech. **89**, 863 (1998).
[19] Z. W. Lu, S. H. Wei, and A. Zunger, Europhys. Lett. **21**, 221 (1993).
[20] Z. W. Lu and A. Zunger, Phys. Rev. B **50**, 6626 (1994).
[21] C. Wolverton and A. Zunger, Comput. Mater. Sci. **8**, 107 (1997).
[22] V. Ozolins, C. Wolverton, and A. Zunger, Phys. Rev. B **57**, 6427 (1998).
[23] C. Wolverton, V. Ozolins, and A. Zunger, Phys. Rev. B **57**, 4332 (1998).
[24] V. Ozolins, C. Wolverton, and A. Zunger, Phys. Rev. B **57**, 4816 (1998).
[25] C. Wolverton, V. Ozolins, and A. Zunger, J. Phys.: Condens. Matter **12**, 2749 (2000).
[26] C. Colinet and A. Pasturel, J. Alloys Compd. **296**, 6 (2000).

[27] Z. W. Lu, S.-H. Wei, A. Zunger, S. Frota-Pessoa, and L. G. Ferreira, Phys. Rev. B **44**, 512 (1991).
[28] Z. W. Lu, S.-H. Wei, and A. Zunger, Phys. Rev. Lett. **66**, 1753 (1991).
[29] Z. W. Lu, S.-H. Wei, and A. Zunger, Phys. Rev. B **44**, 3387 (1991).
[30] Z. W. Lu, S.-H. Wei, and A. Zunger, Phys. Rev. B **45**, 10314 (1992).
[31] N. M. Rosengaard and H. L. Skriver, Phys. Rev. B **49**, 14666 (1994).
[32] Z. W. Lu, B. M. Klein, and A. Zunger, Phys. Rev. Lett. **75**, 1320 (1995).
[33] S. Müller and A. Zunger, Phys. Rev. B **63**, 094204 (2001).
[34] C. Colinet and A. Pasturel, Philos. Mag. A **82**, 1067 (2002).
[35] Z. W. Lu, S.-H. Wei, and A. Zunger, Phys. Rev. B **44**, 10470 (1991).
[36] S. Müller and A. Zunger, Phys. Rev. Lett. **87**, 165502 (2001).
[37] P. Weinberger, C. Blaas, B. I. Bennett, and A. M. Boring, Phys. Rev. B **47**, 10158 (1993).
[38] P. Weinberger, J. Kudrnovsky, J. Redinger, B. I. Bennett, and A. M. Boring, Phys. Rev. B **48**, 7866 (1993).
[39] I. A. Abrikosov and H. L. Skriver, Phys. Rev. B **47**, 16532 (1993).
[40] A. Brown, Acta Crystallogr. **14**, 856 (1961).
[41] J. Kanamori and Y. Kakehashi, J. Phys. (Paris), Colloq. **38**, C-7-274 (1977).
[42] J. B. Darby, Acta Metall. **14**, 265 (1966).
[43] H. F. Hayes and O. Kubaschewski, Met. Sci. J. **5**, 37 (1971).
[44] G. Kresse and J. Furthmüller, Phys. Rev. B **54**, 11169 (1996).
[45] G. Kresse and J. Furthmüller, Comput. Mater. Sci. **6**, 15 (1996).
[46] J. M. Sanchez, F. Ducastelle, and D. Gratias, Physica A **128**, 334 (1984).
[47] A. Zunger, in *Statics and Dynamics of Alloy Phase Transformations*, edited by P. E. A. Turchi and A. Gonis, NATO ASI Series (Plenum Press, New York, 1994), Vol. 319, pp. 361–419.
[48] D. de Fontaine, Solid State Phys. **47**, 33 (1994).
[49] M. H. F. Sluiter and Y. Kawazoe, Phys. Rev. B **71**, 212201 (2005).
[50] R. Kikuchi, Phys. Rev. **81**, 988 (1951).
[51] D. de Fontaine, in *Solid State Physics*, edited by H. Ehrenreich, F. Seitz, and D. Turnbull (Academic Press, New York, 1979), Vol. 34, p. 1.
[52] *Theory and Application of the Cluster and Path Probability Methods*, edited by J. L. Moran-Lopez and J. M. Sanchez (Plenum, New York, 1996).
[53] J. P. Perdew and Y. Wang, Phys. Rev. B **45**, 13244 (1992).
[54] J. P. Perdew, J. A. Chevary, S. H. Vosko, K. A. Jackson, M. R. Pederson, D. J. Singh, and C. Fiolhais, Phys. Rev. B **46**, 6671 (1992).
[55] P. E. Blöchl, Phys. Rev. B **50**, 17953 (1994).
[56] G. Kresse and D. Joubert, Phys. Rev. B **59**, 1758 (1999).
[57] H. J. Monkhorst and J. D. Pack, Phys. Rev. B **13**, 5188 (1976).
[58] M. Methfessel and A. T. Paxton, Phys. Rev. B **40**, 3616 (1989).
[59] T. Mohri, J. M. Sanchez, and D. de Fontaine, Acta Metall. **33**, 1171 (1985).
[60] F. Ducastelle, *Order and Phase Stability in Alloys* (Elsevier Science, New York, 1991).
[61] Z. W. Lu, B. M. Klein, and A. Zunger, Modell. Simul. Mater. Sci. Eng. **3**, 753 (1995).
[62] Z. W. Lu, B. M. Klein, and A. Zunger, J. Phase Equilib. **16**, 36 (1995).
[63] J. M. Sanchez, D. Gratias, and D. de Fontaine, Acta Crystallogr., Sect. A: Cryst. Phys., Diffr., Theor. Gen. Crystallogr. **38**, 214 (1982).
[64] D. de Fontaine, J. Appl. Crystallogr. **8**, 81 (1975).
[65] A. Zunger, S.-H. Wei, L. G. Ferreira, and J. E. Bernard, Phys. Rev. Lett. **65**, 353 (1990).
[66] O. Le Bacq and G. Kresse, unpublished results (2001).
[67] As an example in equiatomic Ag-Pt, without spin-orbit coupling we find, $\Delta E_{L10-L11}$, and ΔE_{40-L11}, of 99.7 and 103.3 meV/atom, respectively, while with spin-orbit coupling these numbers are 102.5 and 104.8 meV/atom.
[68] F. R. de Boer, R. Boom, W. C. M. Mattens, A. R. Miedema, and A. K. Niessen, *Cohesion in Metals, Transition Metal Alloys*, edited by F. R. de Boer and D. G. Pettifor (North-Holland, Amsterdam, 1988).
[69] M. Ellner, J. Less-Common Met. **75**, 5 (1980).
[70] D. G. Pettifor, Solid State Commun. **51**, 31 (1984).
[71] P. Villars, K. Mathis, and F. Hulliger, in *The structures of binary compounds*, edited by F. R. de Boer and D. G. Pettifor (North-Holland, Amsterdam, 1989).
[72] R. A. Johnson, Phys. Rev. B **41**, 9717 (1990).
[73] B. M. Klein, Z. W. Lu, and A. Zunger, in *Statics and Dynamics of Alloy Phase Transformations*, edited by P. E. A. Turchi and A. Gonis, NATO ASI Series (Plenum Press, New York, 1994), Vol. 319, pp. 375.
[74] S. V. Meschel and O. J. Kleppa, J. Alloys Compd. **350**, 205 (2003).
[75] A. Finel, Doctoral Thesis, University of Paris VI, Pierre and Marie Curie (Paris, 1987).
[76] C. Barrett and T. B. Massalski, *Structure of Metals*, 3rd revised ed., *Crystallographic Methods, Principles, and Data*, International Series on Materials Science and Technology (Pergamon Press, Oxford, 1987), Vol. 35.
[77] M. H. F. Sluiter, Y. Watanabe, D. de Fontaine, and Y. Kawazoe, Phys. Rev. B **53**, 6137 (1996).
[78] V. Blum and A. Zunger, Phys. Rev. B **70**, 155108 (2004).
[79] V. Blum and A. Zunger, Phys. Rev. B **69**, 020103(R) (2004).
[80] R. Drautz, R. Singer, and M. Fähnle, Phys. Rev. B **67**, 035418 (2003).
[81] M. H. F. Sluiter and Y. Kawazoe, Phys. Rev. B **68**, 085410 (2003).
[82] G. L. W. Hart, V. Blum, M. J. Walorski, and A. Zunger, Nat. Mater. **4**, 391 (2005).
[83] J. W. D. Connolly and A. R. Williams, Phys. Rev. B **27**, R5169 (1983).
[84] A. Fernandez-Guillermet, V. Ozolins, G. Grimvall, and M. Körling, Phys. Rev. B **51**, 10364 (1995).
[85] A. Pasturel, C. Colinet, D. N. Manh, A. T. Paxton, and M. van Schilfgaarde, Phys. Rev. B **52**, 15176 (1995).
[86] G. D. Garbulsky and G. Ceder, Phys. Rev. B **51**, 67 (1995).
[87] G. Ceder, G. D. Garbulsky, and P. D. Tepesch, Phys. Rev. B **51**, 11257 (1995).
[88] D. A. Vul and D. de Fontaine, in *Material Theory and Modeling*, edited by J. Broughton, P. D. Bristowe, and J. M. Newsam, MRS Symposia Proceedings No. 291 (Materials Research Society, Pittsburgh, 1994), p. 401; Ref. 48, p. 84.
[89] A. van de Walle and G. Ceder, J. Phase Equilib. **23**, 348 (2002).
[90] N. A. Zarkevich and D. D. Johnson, Phys. Rev. Lett. **92**, 255702 (2004).

[91] J. Shao, J. Am. Stat. Assoc. **88**, 486 (1993), as cited in Ref. 78.
[92] M. Sluiter, D. de Fontaine, X. Q. Guo, R. Podloucky, and A. J. Freeman, Phys. Rev. B **42**, 10460 (1990).
[93] P. E. A. Turchi, M. Sluiter, F. J. Pinski, D. D. Johnson, D. M. Nicholson, G. M. Stocks, and J. B. Staunton, Phys. Rev. Lett. **67**, 1779 (1991); **68**, 418 (1992).
[94] M. Sluiter, M. Takahashi, and Y. Kawazoe, J. Alloys Compd. **248**, 90 (1997).
[95] M. Sluiter and Y. Kawazoe, Mater. Trans., JIM **42**, 2201 (2001).
[96] T. Mohri and Y. Chen, Mater. Trans., JIM **43**, 2104 (2002).
[97] Y. Chen, T. Atago, and T. Mohri, J. Phys.: Condens. Matter **14**, 1903 (2002).
[98] A. Zunger, L. G. Wang, G. L. W. Hart, and M. Sanati, Modell. Simul. Mater. Sci. Eng. **10**, 685 (2002).
[99] A. Bieber, F. Gautier, G. Treglia, and F. Ducastelle, Solid State Commun. **39**, 149 (1981).
[100] M. Sluiter, P. E. A. Turchi, F. J. Pinski, and G. M. Stocks, Mater. Sci. Eng., A **152**, 1 (1992).
[101] M. Sluiter, Comput. Mater. Sci. **2**, 293 (1994).
[102] R. Hultgren, P. Desai, D. Hawkins, M. Gleiser, and K. Kelley, *Selected Values of the Thermodynamic Properties of Binary Alloys* (ASM, Metals Park, OH, 1973).
[103] R. Höhn and C. Herzig, Z. Angew. Math. Mech. **77**, 291 (1986).
[104] J. Tomiska, Z. Angew. Math. Mech. **81**, 912–918 (1990).
[105] M. Sluiter and Y. Kawazoe, Europhys. Lett. **57**, 526 (2002).
[106] A. van de Walle and G. Ceder, Rev. Mod. Phys. **74**, 11 (2002).
[107] E. J. Wu, G. Ceder, and A. van de Walle, Phys. Rev. B **67**, 134103 (2003).
[108] M. H. F. Sluiter, V. Vinograd, and Y. Kawazoe, Phys. Rev. B **70**, 184120 (2004).
[109] A. Nagasawa, Y. Matsuo, and J. Kakinoki, J. Phys. Soc. Jpn. **20**, 1881 (1965).
[110] Y. Matsuo, A. Nagasawa, and J. Kakinoki, J. Phys. Soc. Jpn. **21**, 2633 (1966).
[111] Y. Kawasaki, S. Ino, and S. Ogawa, J. Phys. Soc. Jpn. **30**, 1758 (1971).
[112] A. Maeland and T. B. Flanagan, Can. J. Phys. **42**, 2364 (1964).
[113] V. I. Iveronovna and A. A. Katsnelson, Sov. Phys. Crystallogr. **9**, 467 (1964).
[114] W. Lin, J. E. Spruiell, and R. O. Williams, J. Appl. Crystallogr. **3**, 297 (1970).
[115] H. P. R. Frederikse, in *CRC Handbook of Chemistry and Physics*, 85th ed. (CRC Press, Boca Raton, Fl., 2004), pp. 12–35.